Geophysical Research Letters

RESEARCH LETTER
10.1029/2019GL083816

Extreme Conditions in the Bering Sea (2017–2018): Record-Breaking Low Sea-Ice Extent

Phyllis J. Stabeno[1] and **Shaun W. Bell**[1,2]

[1]NOAA Pacific Marine Environmental Laboratory, Seattle, WA, USA, [2]JISAO, University of Washington, Seattle, WA, USA

Key Points:
- Wind patterns have changed in the Bering Sea, with a marked increase in warm southerly winds since 2016
- These changes in winds have resulted in decrease in sea ice, with the lowest extent ever observed in the Bering Sea occurring in 2017/2018
- The low ice extent restructured the horizontal temperature patterns, resulting in an almost nonexistent cold pool in August 2018

Correspondence to:
P. J. Stabeno,
phyllis.stabeno@noaa.gov

Citation:
Stabeno, P. J., & Bell, S. W. (2019). Extreme conditions in the Bering Sea (2017–2018): Record-breaking low sea-ice extent. *Geophysical Research Letters*, *46*, 8952–8959. https://doi.org/10.1029/2019GL083816

Received 23 MAY 2019
Accepted 30 JUN 2019
Accepted article online 7 AUG 2019
Published online 14 AUG 2019

Abstract The lowest winter-maximum areal sea-ice coverage on record (1980–2019) in the Bering Sea occurred in the winter of 2017/2018. Sea ice arrived late due to warm southerly winds in November. More typical northerly winds (albeit warm) in December and January advanced the ice, but strong, warm southerlies in February and March forced the ice to retreat. The cold pool (shelf region with bottom water < 2 °C) was the smallest on record, because of two related mechanisms: (1) lack of direct cooling in winter by melting sea ice and (2) weaker vertical stratification (no ice melt reduced the vertical salinity gradient) allowing surface heating to penetrate into the near bottom water during summer. February 2019 exhibited another outbreak of warm southerly winds forcing ice to retreat. The number of >31-day outbreaks of southerly winds in winter has increased since 2016.

1. Introduction

The Bering Sea is an Arctic system with sea ice typically appearing in late October or early November and persisting into June. Ice forms in polynyas along the coast of Siberia and Alaska and in the lee of islands. This ice is then advected southward over the eastern shelf, with the leading-edge melting and cooling the water column (Pease, 1980). Maximum sea-ice extent has occurred as early as January and late as April but more typically in late March (Stabeno, Farley, et al., 2012; Stabeno, Kachel, et al., 2012). The advance of ice is primarily dependent upon atmospheric forcing and to a smaller degree on ocean temperatures. Strong frigid northerly winds directly cool the water column, form ice in polynyas, and drive it southward across the shelf. Although warm ocean water can delay the advance of ice, persistent cold northerly winds will eventually cool (radiative heat flux and ice melt) the water column sufficiently to push sea ice southward.

The eastern Bering Sea (EBS) shelf is divided at ~60°N between the northern (herein used to indicate the region north of 60°N and east of 178°E) and southeastern Bering Sea (SEBS; Stabeno, Kachel, et al., 2012). Prior to 2015, the northern Bering Sea (NBS) was largely ice covered for ~5 months each year. In contrast, sea-ice extent in the SEBS is more variable, with ice in some years (e.g., 2012; Figure 1a) extending southward to the Alaska Peninsula and westward beyond the slope, and in other years, the southern shelf is largely ice-free (e.g., 2003; Figure 1a). In the vicinity of M8, the NBS experiences considerable variability (standard deviation = 25 days) in the timing of ice arrival/retreat, but from 1979 to 2015, there was no significant trend in these variables (Stabeno et al., 2018). In contrast, the SEBS was dominated by year-to-year variability prior to 2000 and, since then, has been dominated by alternating stanzas of extensive ice and cold temperatures (2007–2013) and minimal ice and warm ocean temperatures (2001–2005 and 2014–2018; Stabeno, Kachel, et al., 2012, Stabeno et al., 2018). While in the long run, the increased atmospheric CO_2 and warming earth will result in loss of much of the ice in the Bering Sea (Wang & Overland, 2009), this magnitude of loss was not expected until the 2030s. Recent years put this prediction in question (Stabeno et al., 2018; Wang et al., 2018). During three of the last four years (2014/2015, 2016/2017, and 2017/2018), ice in the NBS has arrived later and retreated earlier, resulting in a significantly shorter ice season (Stabeno et al., 2018). In this manuscript, we examine extremes in sea-ice extent during the 2017/2018 and 2018/2019 ice seasons, focusing on data from two long-term moorings, M5 and M8, in the EBS north of 59.9°N (Figure 1a).

2. Data Sources and Methods

North American Regional Reanalysis, a regional enhancement of the National Center for Environmental Prediction reanalysis (Kalnay et al., 1996; Mesinger et al., 2006), provides data from January 1979 to

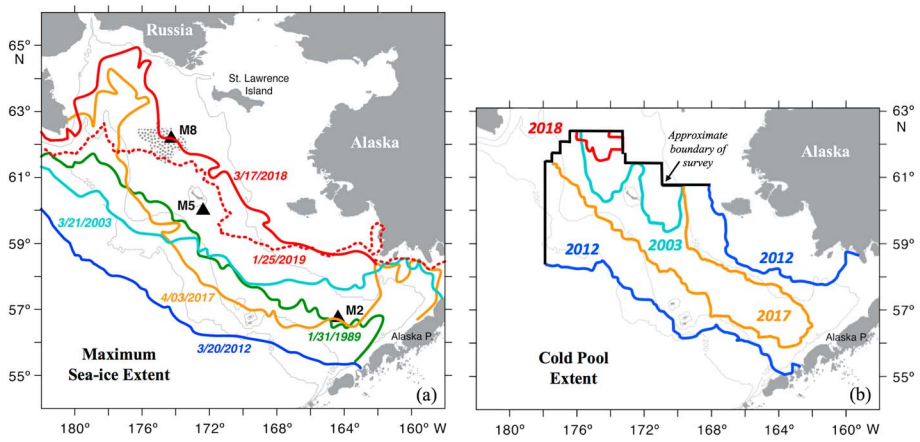

Figure 1. (a) Maximum sea-ice extent in the eastern Bering Sea for selected years and mooring locations (M2, M5, and M8). The black dotted area indicates 2018 cold-pool extent shown in (b). (b) The extent of the cold pool for the same years as in (a), except for 1989 for which limited data were available. Cold-pool data came from National Marine Fisheries Service Bottom Trawl Survey.

March 2019 from the high-resolution Eta model using the Regional Data Assimilation System. North American Regional Reanalysis wind and temperature data were obtained from NOAA, Boulder, Colorado, United States (https://www.esrl.noaa.gov/psd/).

Sea-ice concentration data were retrieved from National Snow and Ice Data Center (http://nsidc.org/data/nsidc-0079 or http://nsidc.org/data/nsidc-0081). The daily version 3 bootstrap Sea-Ice Concentrations (Comiso, 2017) was available for the period October 1978–December 2017. Version 1 Near-Real-Time Sea-Ice Concentrations (Maslanik & Stroeve, 1999) was used to extend the data set through March 2019.The EBS Ice Extent product used in this manuscript is defined in the same manner as the Regional Sea-Ice Extent, V3 product (National Snow and Ice Data Center; Fetterer et al., 2017) but limited to the area east of 178°E (Figure 1).

Three mooring sites are discussed here: M2 (56.87°N, 164.05°W) first deployed in 1995, and M5 (59.92°N, 171.73°W) and M8 (62.19°N, 174.69°W) first deployed in 2005. For details of the moorings, see Stabeno, Kachel, et al. (2012).

Bottom temperature (±0.1 °C) data are collected as part of the National Marine Fisheries Service bottom trawl surveys (Buckley et al., 2009; Stauffer, 2004) on ~37-km grid on the EBS shelf (Figure 1b).

3. Results and Discussion

3.1. Spatial Patterns of Sea Ice and the Cold Pool

In extensive sea-ice years, ice can cover virtually the entire EBS shelf (e.g., 2012; Figure 1a), but even in years with limited ice (e.g., 2003), it still covers much of the northern shelf. That is, until 2018, when ice extent was at record lows for almost the entire winter (Figure 2a).

Sea-ice extent in late winter and spring determines the extent of the cold pool (Wyllie-Echeverria & Wooster, 1998) that region of the EBS shelf where bottom waters are <2 °C through summer (Figure 1b). This relationship is evident in the ice and cold pool extents shown in Figure 1. For instance, 2012 with its extensive ice is associated with the most extensive cold pool (Figures 1 and 2a). In contrast, 2018, with minimal ice, had an almost nonexistent cold pool in the Bering Sea. It is interesting to note that contrary to the August cold-pool extent in the SEBS, which is only found beneath maximum sea-ice extent, that part of the cold pool in 2018 was outside the maximum sea-ice extent (Figure 1a). That is, at least in the NBS, it appears that cold atmospheric conditions can cool the water column sufficiently for a cold pool to persist into August (see section 3.3 for additional discussion).

In summer, the cold pool is primarily found in the middle shelf domain (water depth 50–100 m) of the EBS, which is usually well mixed during winter and two-layered during summer (Stabeno, Farley,

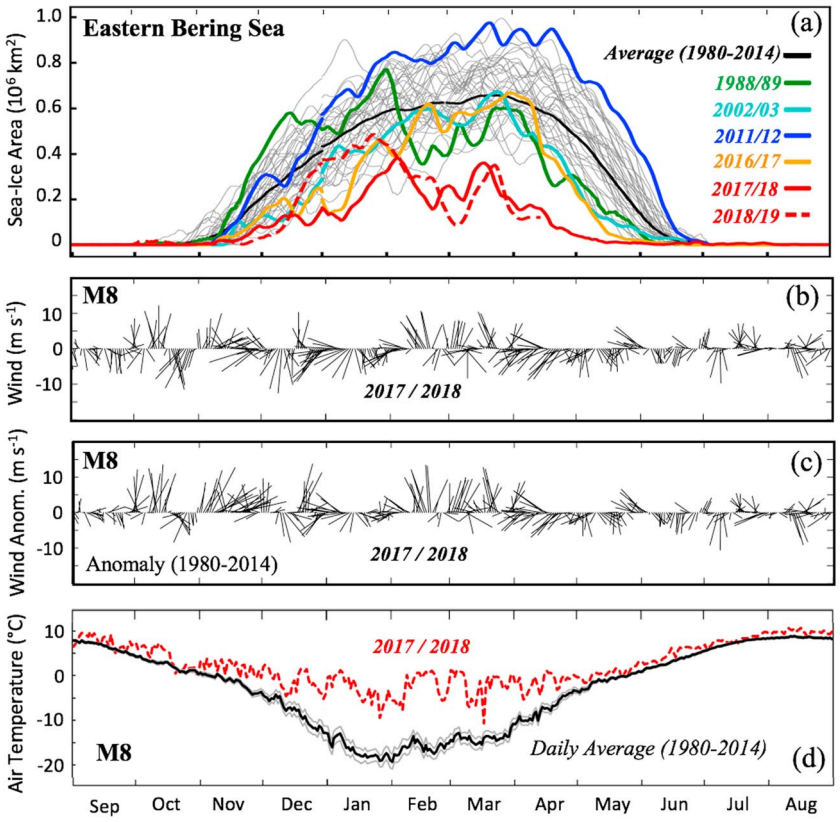

Figure 2. (a) Areal ice cover in the eastern Bering Sea for 1980–2019. Most years are in gray; years in Figure 1 are in colors. Black indicates the long-term daily mean (1980–2014). (b) Wind and (c) wind anomalies for September 2017 to August 2018 at M8. A 3-day running mean was applied to both time series for clarity. Up indicates northward winds. (d) Atmospheric temperature at M8 (red) for 2017–2018 and daily mean (black; 1980–2014) atmospheric temperature. Gray indicates the standard error of the mean.

et al., 2012; Stabeno, Kachel, et al., 2012). The strong stratification below the surface wind-mixed layer isolates the bottom layer from atmospheric heating, allowing it to remain cold until seasonal mixing occurs in late summer/early fall (Stabeno et al., 2018). The cold pool is important in structuring the Bering Sea ecosystem (e.g., Mueter & Litzow, 2008). It acts as a barrier for adult subarctic fishes such as pollock (*Gadus chalcogrammus*) and Pacific cod (*Gadus macrocephalus*; Boldt et al., 2012; Ciannelli & Bailey, 2005), a refuge for young-of-the-year pollock (Duffy-Anderson et al., 2017), and a corridor for Arctic species such as Arctic cod (*Boreogadus saida*) and zooplankton (e.g., *Calanus glacialis*) to migrate into SEBS.

3.2. Causes of the 2017/2018 Low Ice Extent

As previously mentioned, sea-ice advance is forced by frigid (less than −5 °C) winds out of the north. Historically, such winds dominate during November–March (Figure 3). Winds in the Bering Sea during much of the 2017/2018 ice season, however, were highly unusual and fall into four periods (Figures 2c and 3). In November, warm northward winds delayed the arrival of ice on the northern shelf (Figure 2). Wind direction in the following two months, December and January, was out of the north and northeast, which is typical, but was >5 °C warmer than usual (Figures 2b–2d). This supported a weak ice advance with relatively thin ice (Thompson, 2018). Conditions in February through mid-March changed radically. Winds shifted from northerlies to southerlies, and air temperatures warmed. These unusual and persistent winds drove the ice northward and reduced the areal coverage to <40% of normal (Figures 2a–2c and 3). Wind direction was relatively normal in late March through May, but warm ocean temperatures, above average air temperatures and the beginning of spring heating, limited ice advance.

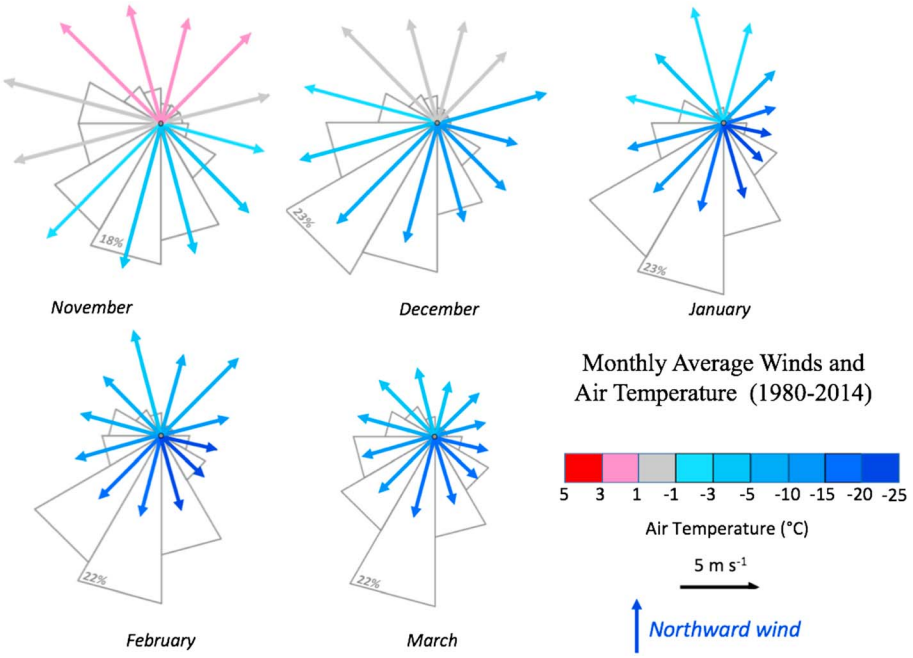

Figure 3. Radial histogram of winds (>2 m/s) in 12 equal, 30° sectors (e.g., 0–30° and 30–60°). Gray indicates the percent of time winds are in that sector. The vectors are the mean wind in that sector, color-coded by the mean air temperature when winds are in that sector.

On the EBS shelf, winds drive the ice ~40° to the right of the wind direction (Macklin et al., 1984; Sullivan et al., 2014). Therefore, wind direction ranging between 165° (approximately west-northwestward) and 30° (approximately east-northeastward) is optimum for pushing ice toward the Russian and/or the Alaskan coasts, thus reducing areal ice extent. Here we use the mathematical convention with 90° indicating northward and 0° eastward.

In the following, we quantify the atmospheric conditions from 1980 through March 2019 to demonstrate how unusual the 2017/2018 ice season was. A centered 31-day running mean was applied to the daily wind-vectors (W) and air-temperature time series. We then extracted the ice-formation seasons (November through March each year) from the vector time series, creating a new time series (W_{31}). There were only 228 (out of a possible >6,000) wind vectors in W_{31} when wind direction fell within the arc of 165–30° (referred to as $A_{30–165}$ herein). (Adjacent points in W_{31} overlap by 30 days and are not independent.) These 228 wind vectors self-organize into 13 unique sets (Table 1). Except for Partition 12 (P12), each partition consists of consecutive vectors with wind direction toward $A_{30–165}$. In P12, there were five consecutive points where the direction ranged from 166° to 170°, slightly outside sector $A_{30–165}$.

The number of days in each partition (P1–P13) is the number of W_{31} points with northward ($A_{30–165}$) winds plus 30 days (size of the filter). Of the points in the union of the partitions P1–P13, 40% of the days (W) have daily winds toward $A_{30–165}$; within only five partitions (P1, P4, P9, P12, and P13) did it exceed 40%. Second, in only five periods (P1, P5, P9, P11, and P12) was the mean wind direction toward sector $A_{30–165}$, although, mean wind in P13 was just 3° outside the sector. Thus, there are three periods (P1, P9, and P12) that fall into both categories, indicating persistence. Air temperatures generally were dependent upon month with the coldest temperatures (e.g., P2) occurring primarily in winter and the warmest (e.g., P3) in November.

Each of the periods (P1–P13) was associated with significant sea-ice retreat or, in the case of P3 and P4, delayed ice arrival (Table 1). The magnitude of ice retreat was dependent upon two factors: the strength/duration of southerly winds and how much ice was present. The partition with highest percentage of retreat was P13, when January ice extent was near normal and persistent northward winds in February forced an extensive ice retreat. The three other highest percentages of ice retreat occurred in years with the most persistent northward winds (P1, P9, and P12). The largest areal retreat was P1 when there was extensive ice prior to the northward wind event.

Table 1
Timing of Wind Events (Partitions) When There Was at Least One 31-Day Centered-Averaged Wind Event (W_{31}) Toward $A_{30–165}$

Part	Date total period	Total # of days	Number of days toward $A_{30–165}$	AT ± STD (°C)	Average wind velocity: Overall speed (Dir) (m s^{-1}(°))	Average wind velocity: Toward A_{30-165} Speed (Dir) (m s^{-1}(°))	Max ice extent (km^2) (% decrease)
P1	**1/29/1989–3/10/1989**	**71**	**35**	**−10.6 ± 10.7**	**1.9 (157[a])**	**4.3 (115)**	**770,717 (54)**
P2	12/26/1992–1/23/1993	59	18	−15.9 ± 10.9	0.8 (173)	5.6 (103)	536,374 (31)
P3	11/2/1996–11/11/1996	39	13	1.7 ± 2.0	4.0 (−178)	9.2 (116)	
P4	**11/8/2003–11/12/2003**	**35**	**16**	**1.4 ± 3.2**	**0.4 (172)**	**5.5 (97)**	
P5	12/20/2003–12/21/2003	32	12	−1.9 ± 3.5	5.0 (163[a])	9.3 (123)	361,374 (23)
P6	2/14/2006–3/1/2006	45	17	−12.9 ± 8.4	1.1 (−165)	3.0 (109)	817,162 (38)
P7	2/28/2009–3/6/2009	37	11	−13.3 ± 7.7	0.3 (−87)	4.1 (101)	789,331 (31)
P8	2/8/2011–3/7/2011	57	20	−13.8 ± 6.8	1.0 (174)	3.9 (108)	680,552 (24)
P9	**12/18/2016–12/30/2016**	**42**	**21**	**0.0 ± 2.8**	**4.2 (160[a])**	**8.8 (116)**	**250,140 (45)**
P10	3/9/2017–3/11/2017	33	10	−9.5 ± 5.1	1.1 (170)	3.9 (107)	618,739 (20)
P11	11/11/2017–11/24/2017	43	17	1.6 ± 1.4	0.6 (95[a])	6.7 (92)	19,901 (21)
P12	**2/6/2018–3/21/2018**	**74**	**36**	**−2.7 ± 2.9**	**2.2 (154[a])**	**6.6 (103**	**381,080 (42)**
P13	**2/6/2019–3/3/2019**	**56**	**26**	**−5.9 ± 6.2**	**2.7 (168)**	**6.9 (119)**	**486,023 (82)**

Note. Listed are the total number of days in each partition, the number of individual nonfiltered days (W) on which the wind direction was toward $A_{30–165}$, the average air temperature (AT) and standard deviation (STD) during the total period, the average wind velocity during the total period, and average wind velocity on individual days (W) when wind was toward $A_{30–165}$ (90° is northward). Bold indicates those partitions when the ($A_{30–165}$ days) (total days) is greater than the average (40%). The final column is maximum areal ice extent and percent decrease during the total period. P3 and P4 had negligible ice extent (<2,000 km^2).
[a]Those partitions when average wind direction of the total days is toward $A_{30–165}$.

The atmospheric forcing in 2017/2018 ice season was unique in that (1) there were two periods (P11 and P12) with persistent winds toward $A_{30–165}$, (2) it had the most individual days with winds (W) toward $A_{30–165}$ (53), and (3) air temperatures were relatively warm (Table 1). Ice year 2018/2019 was most similar to 2017/2018, but there was a quantifiable difference; winds in November 2018 through January 2019 were cold and out of the north, so that areal ice extent was just below average in January 2019 (Figure 2a). The only other year that was comparable to 2017/2018 and 2018/2019 was 1988/1989, when (1) like 2018/2019 cold, southward winds dominated in November through January, (2) southerly winds in 29 January to 10 March 1989 (P1) were persistent but weaker than those in 2018 (P12) and 2019 (P13), and (3) air temperatures were much colder. These colder winds, while moving the ice northward, would be less likely to contribute to melting. Finally, when winds returned to northerlies in mid-March 1989, the ocean was relatively cold (preconditioned by ice in January 1989) allowing ice to be advected southward without substantial melting. In March 2018 and 2019, ice had been limited to the northern shelf, and so warm (>1 °C) water delayed any southward advance of ice in late March and April. The record-breaking low-ice extent in 2018 was a result of two factors: (1) delayed ice formation because of strong southerly winds in November and (2) strong persistent warm winds out of the south for 36 days in February and March (Table 1).

The double (P11 and P12) occurrence of southerly winds in 2017–2018 may be related to changes in the temporal occurrence of these month-long outbreaks of southerly winds. Prior to 2016, such atmospheric patterns occurred every 3 years or so, and since 2016, it has happened five times (Table 1).

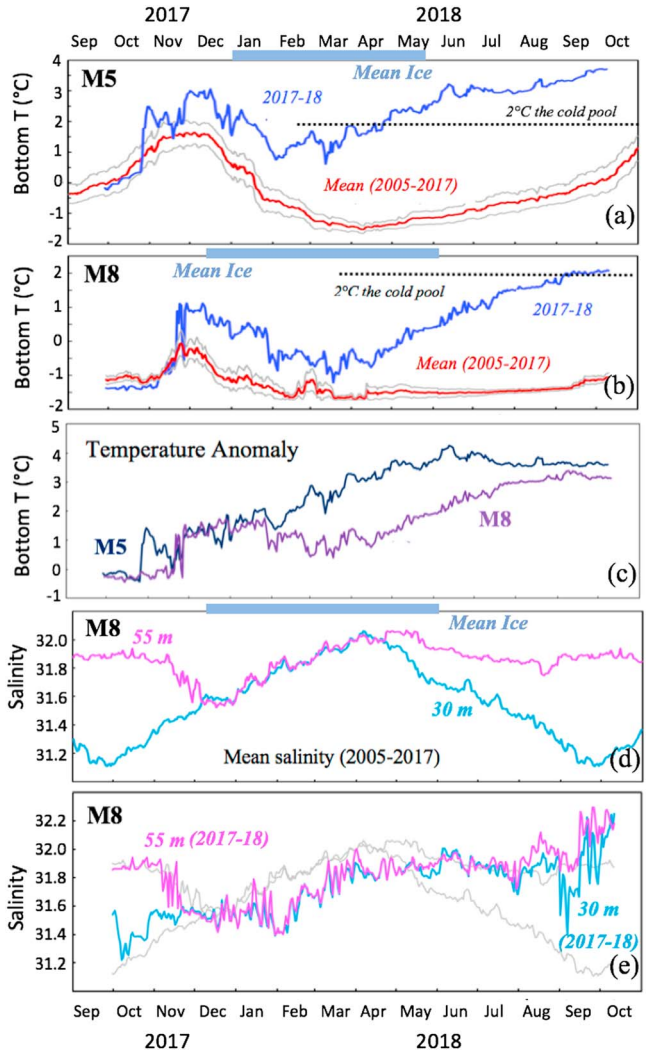

Figure 4. The average near-bottom (10- to 15-m off bottom; 2005–2017) temperature (red) and 2017–2018 time series (blue) at (a) M5 and (b) M8. The gray lines indicate the standard error of the mean. (c) Near-bottom temperature anomalies. (d) The annual mean signal of salinity at M8 (2005–2017) at 30 and 55 m. (e) The salinities at M8 during 2017–2018 (colored lines) and mean salinity from (d) (gray). The thick blue lines (a, b, d) indicate annual average (1979–2014) presence of >20% areal sea-ice cover in 50 km × 50 km box centered on each mooring.

3.3. The Cold Pool and the Seasonal Cycle of Temperature and Salinity

To examine the cold pool in more detail, we focus on two moorings: M5 near St. Matthew Island and M8 southwest of St. Lawrence Island. On average (1980–2017), areal sea-ice concentration in a 50 km × 50 km box centered on M8 exceeds 20% in mid-December through early June (thick blue line Figure 4b). At M5, ice arrives later in late December and retreats earlier by middle to late May. At both sites, average (2005–2017) bottom ocean temperatures were the coldest (approximately −1.7 °C) in March/April, with M5 remaining <0 °C through September and M8 throughout the year. With the arrival of seasonal cooling and fall storms, the water column mixes, and bottom temperatures reach a maximum in November or December. Finally, winter cooling and the arrival of sea ice reduce ocean temperatures to −1.7 °C, which is maintained through winter (Figures 4a and 4b).

At both sites, ocean temperatures in mid-October 2017 were fairly typical, but by December, bottom temperature anomalies were >1 °C. Bottom temperatures then began to cool reaching a minimum in March. During this cooling period, both sites would typically be ice covered (Figures 4a and 4b). At M5, the bottom temperature anomalies increased from December to June (Figure 4c), with bottom temperatures rising above 2 °C (cold-pool threshold) in April (Figure 4a). At M8, bottom anomalies increased from April through August (Figure 4c), with bottom temperatures rising above 2 °C in late August (Figure 4b). That temperature anomalies remained above average in winter and spring was likely due to the lack of ice. The atmosphere cools the water column to ~0 °C, but in the SEBS, the final cooling to below −1.7°C generally requires melting ice (Stabeno, Kachel, et al., 2012; Sullivan et al., 2014). The most likely causes of summer warming are advection of warmer water from the south and/or weakened vertical stratification that allowed vertical mixing of heat from the surface.

Advective warming has been observed at M5 (Stabeno et al., 2016; Stabeno, Kachel, et al., 2012) but not at M8 where the flow is weaker. Lack of warming of bottom water at M8 is evident in relatively constant mean temperature in Figure 4b during summer. In 2018, however, the north-south ocean temperature gradient was larger so advective warming cannot be ruled out. A more likely cause, however, for warming during summer was weaker stratification.

Vertical stratification over the middle shelf is strong and acts as a barrier to warming of bottom water during summer months. In the NBS (M8), vertical stratification in summer is due to equal parts temperature and salinity (Stabeno, Farley, et al., 2012). The low salinity surface water results from melting ice in spring. Relatively weak May winds cannot mix the entire water column over the middle shelf, resulting in a surface lens of low salinity (~30) water overlaying the more saline (~32) bottom water. Thus, the two-layer structure on the NBS shelf in June-September is characterized by warm, fresher surface wind-mixed layer (~20 m deep) and a cold, more saline bottom tidally mixed layer (~30 m).

The salinity structure at M8 in 2018 was highly unusual (Figures 4d and 4e). Only in fall 2017 did salinity contribute to vertical stratification. There was no ice in the 50 km × 50 km box centered at M8 in fall 2017 and 5 days of ice in 2018 (only 17 March at 17% had areal ice cover >10%). In the box around M5, there was no ice from November 2017 to May 2018. This limited ice, and hence ice melt, at M8 in spring 2018 resulted in minimal low-salinity water in the near surface and, thus, halving the strength of the vertical stratification. This weaker stratification allowed warming of the bottom throughout summer.

The data from these mooring sites indicate that earlier in summer, a cold pool existed over parts of the NBS shelf. The bottom survey samples in late summer and by that time the cold pool had shrunk substantially.

4. Summary and Conclusions

Historically, ice duration/arrival in the NBS has been dominated by high year-to-year variability with no trend. The changes observed during the last 4 years fall within changes predicted to occur before 2030—ice retreating earlier and arriving later, resulting in an annual decrease in ice duration of 20–30 days (Wang et al., 2018).

Events of persistent winds out of the south have occurred 13 times in 40 years but have occurred five times since 2016. February and March ice extent in 2018 and 2019 were the lowest on record. Models have predicted that southerly winds will increase over next decades (Hermann et al., 2019), and we may be seeing the beginning of such a shift.

Winter, near-bottom ocean temperatures were the warmest on record at M5 and M8 in 2018 (the 2019 data are not yet available). In contrast, a record maximum did not occur on the SEBS in 2018. The depth-averaged temperatures at M2 (Stabeno et al., 2017) are the highest in August. In 2018, the depth-averaged August temperature was 6.6 °C, which was similar (±0.1 °C) to what occurred in 2005, 2014, and 2015 and ~1.2 °C cooler than observed in 2016. All of these years were classified as warm years with ice limited to the northern shelf. Temperatures in 2016 were warmer than 2018 likely because previous years had also been warm, thus providing a remnant of heat (Stabeno et al., 2017).

What does the future hold? Lower ice concentrations caused by southerly winds in winter appear to be more common, but variability in ice extent also has increased. For instance, the most extensive ice occurred in 2012 (Figure 2a), but just 6 years later, the least extensive ice was observed—a large swing from cold to warm. The SEBS has been dominated by multiyear patterns of warm/ice-free stanzas versus cold/extensive-ice stanzas. Perhaps NBS is experiencing such variability.

Changes in the timing of sea-ice arrival/retreat and extent directly impact the ecosystem beyond the physics. These impacts include the timing of the spring bloom, zooplankton abundance, and survival of young pollock. It also impacts the coastal communities of the NBS, where residents depend on sea ice for travel during winter, as a platform for whaling and hunting and to protect coastal infrastructure from winter storm surges (https://www.climate.gov/news-features/features/coastal-communities-near-bering-strait-winter-unlike-rest).

Acknowledgments
This research is contribution 4908 from NOAA/Pacific Marine Environmental Laboratory and 0923 from NOAA's Ecosystems Fisheries Oceanography Coordinated Investigations. Data used for bottom temperature at M5 and M8 are available as compressed NetCDF files via the NOAA, EcoFOCI web site (https://www.pmel.noaa.gov/foci/data/data.html). Additionally, a subset of these data is available at the Arctic Data Center (NSF) and UCAR/EOL data archive. Data submittal is pending on NOAA/PMEL ERDDAP data server (search PMEL EcoFOCI Bering Sea). This publication is primarily funded by NOAA and partially funded by Joint Institute for the Study of the Atmosphere and Ocean, University of Washington (NOAA Cooperative Agreement NA10OAR4320148). The research was also supported by grants from the North Pacific Research Board (517, 602, 701, 1302, and B52). This manuscript was greatly improved by comments from three anonymous reviewers.

References

Boldt, J. L., Buckley, T. W., Rooper, C. N., & Aydin, K. (2012). Factors influencing cannibalism and abundance of walleye pollock (*Theragra chalcogramma*) on the eastern Bering Sea shelf, 1982–20. *Fishery Bulletin*, *110*(3), 293–306.

Buckley, T. W., Greig, A., & Boldt, J. L. (2009). *Describing summer pelagic habitat over the continental shelf in the eastern Bering Sea, 1982-2006 (NOAA Tech. Memo. NMFS-AFSC-196)*. Washington, DC: U.S. Department of Commerce.

Ciannelli, L., & Bailey, K. M. (2005). Landscape dynamics and resulting species interactions: The cod-capelin system in the southeastern Bering Sea. *Marine Ecology Progress Series*, *291*, 227–236. https://doi.org/10.3354/meps291227

Comiso, J. C. (2017). *Bootstrap sea ice concentrations from Nimbus-7 SMMR and DMSP SSM/I-SSMIS, version 3*. Boulder, CO: NASA National Snow and Ice Data Center Distributed Active Archive Center, Boulder, CO. https://doi.org/10.5067/7Q8HCCWS4I0R Accessed 2017

Duffy-Anderson, J. T., Stabeno, P. J., Siddon, E. C., Andrews, A. G., Cooper, D. W., Eisner, L. B., et al. (2017). Return of warm conditions in the southeastern Bering Sea: Phytoplankton – fish. *PLoS ONE*, *12*(6), e0178955. https://doi.org/10.1371/journal.pone.0178955

Fetterer, F., Knowles, K., Meier, W., Savoie, M., & Windnagel, A. K. (2017). updated daily. Sea Ice Index, Version 3. [Bering Sea Extent]. Boulder, CO. NSIDC: National Snow and Ice Data Center. https://doi.org/10.7265/N5K072F8 [2019-02-07].

Hermann, A. J., Gibson, G. A., Cheng, W., Ortiz, I., Aydin, K., Wang, M., et al. (2019). Projected biophysical conditions of the Bering Sea to 2100 under multiple emission scenarios. *ICES Journal of Marine Science*, fsz043. https://doi.org/10.1093/icesjms/fsz043

Kalnay, E., Kanamitsu, M., Kistler, R., Collins, W., Deaven, D., Gandin, L., et al. (1996). The NCEP/NCAR 40-Year Reanalysis Project. *Bulletin of the American Meteorological Society*, *77*(3), 437–471. https://doi.org/10.1175/1520-0477(1996)077<0437:TNYRP>2.0.CO;2

Macklin, S. A., Pease, C. H., & Reynolds, R. M. (1984). *Bering Air-Sea-Ice Study (BASICS), February and March 1981 (NOAA Tech Memo ERL PMEL-52)*. Washington, DC: U.S. Department of Commerce.

Maslanik, J., & Stroeve, J. (1999, updated daily). Near-real-time DMSP SSMIS daily polar gridded sea ice concentrations, version 1. Boulder, CO: NASA National Snow and Ice Data Center Distributed Active Archive Center. https://doi.org/10.5067/U8C09DWVX9LM [Accessed 2018]

Mesinger, F., DiMego, G., Kalnay, E., Mitchell, K., Shafran, P. C., Ebisuzaki, W., et al. (2006). North American Regional Reanalysis. *Bulletin of the American Meteorological Society*, *87*(3), 343–360. https://doi.org/10.1175/BAMS-87-3-343

Mueter, F. J., & Litzow, M. A. (2008). Sea ice retreat alters the biogeography of the Bering Sea continental shelf. *Ecological Applications*, *18*(2), 309–320. https://doi.org/10.1890/07-0564.1

Pease, C. H. (1980). Eastern Bering Sea ice processes. *Monthly Weather Review*, *108*(12), 2015–2023. https://doi.org/10.1175/1520-0493(1980)108<2015:EBSIP>2

Stabeno, P. J., Bell, S. W., Bond, N. A., Kimmel, D. G., Mordy, C. W., & Sullivan, M. E. (2018). Distributed biological observatory region 1: Physics, chemistry and plankton in the northern Bering Sea. *Deep Sea Research Part II: Topical Studies in Oceanography*, *162*, 8–21. https://doi.org/10.1016/j.dsr2.2018.11.006

Stabeno, P. J., Danielson, S., Kachel, D., Kachel, N. B., & Mordy, C. W. (2016). Currents and transport on the eastern Bering Sea shelf: An integration of over 20 years of data. *Deep Sea Research Part II: Topical Studies in Oceanography*, *134*, 13–29. https://doi.org/10.1016/j.dsr2.2016.05.010

Stabeno, P. J., Duffy-Anderson, J. T., Eisner, L. B., Farley, E. V., Heintz, R. A., & Mordy, C. W. (2017). Return of warm conditions in the southeastern Bering Sea: Physics to fluorescence. *PLoS One*, *12*(9), e0185464. https://doi.org/10.1371/journal.pone.0185464

Stabeno, P. J., Farley, E., Kachel, N., Moore, S., Mordy, C., Napp, J. M., et al. (2012). A comparison of the physics of the northern and southern shelves of the eastern Bering Sea and some implications for the ecosystem. *Deep Sea Research Part II: Topical Studies in Oceanography*, *65-70*, 14–30. https://doi.org/10.1016/j.dsr2.2012.02.019

Stabeno, P. J., Kachel, N. B., Moore, S. E., Napp, J. M., Sigler, M., Yamaguchi, A., & Zerbini, A. N. (2012). Comparison of warm and cold years on the southeastern Bering Sea shelf and some implications for the ecosystem. *Deep Sea Research Part II: Topical Studies in Oceanography*, *65-70*, 31–45. https://doi.org/10.1016/j.dsr2.2012.02.020

Stauffer, G. (2004). *NOAA protocols for groundfish bottom trawl surveys of the nation's fishery resources. (Technical Memorandum NMFS-F/SPO-65)*. Washington DC: US Department of Commerce, NOAA, USA.

Sullivan, M. E., Kachel, N. B., Mordy, C. W., Salo, S. A., & Stabeno, P. J. (2014). Sea ice and water column structure on the eastern Bering Sea shelf. *Deep Sea Research Part II: Topical Studies in Oceanography*, *109*, 39–56. https://doi.org/10.1016/j.dsr2.2014.05.009

Thompson, A. (2018). Shock and thaw—Alaskan sea ice just took a steep, unprecedented dive, Scientific American, May 2, 2018.

Wang, M., & Overland, J. E. (2009). A sea ice free summer Arctic within 30 years? *Geophysical Research Letters*, *36*, L07502. https://doi.org/10.1029/2009GL037820

Wang, M., Yang, Q., Overland, J. E., & Stabeno, P. J. (2018). Sea-ice cover timing in the Pacific Arctic: The present and projections to mid-century by selected CMIP5 models. *Deep Sea Research Part II: Topical Studies in Oceanography*, *152*, 22–34. https://doi.org/10.1016/j.dsr2.2017.11.017

Wyllie-Echeverria, T., & Wooster, W. S. (1998). Year-to-year variations in Bering Sea ice cover and some consequences for fish distribution. *Fisheries Oceanography*, *7*(2), 159–170. https://doi.org/10.1046/j.1365-2419.1998.00058.x